Femtosecond laser-induced phase transformations in amorphous Cu77Ni6Sn10P7 alloy

Y. Zhang, L. Liu, G. Zou, N. Chen, A. Wu, H. Bai, and Y. Zhou

Citation: Journal of Applied Physics **117**, 023109 (2015); doi: 10.1063/1.4905588
View online: http://dx.doi.org/10.1063/1.4905588
View Table of Contents: http://scitation.aip.org/content/aip/journal/jap/117/2?ver=pdfcov
Published by the AIP Publishing

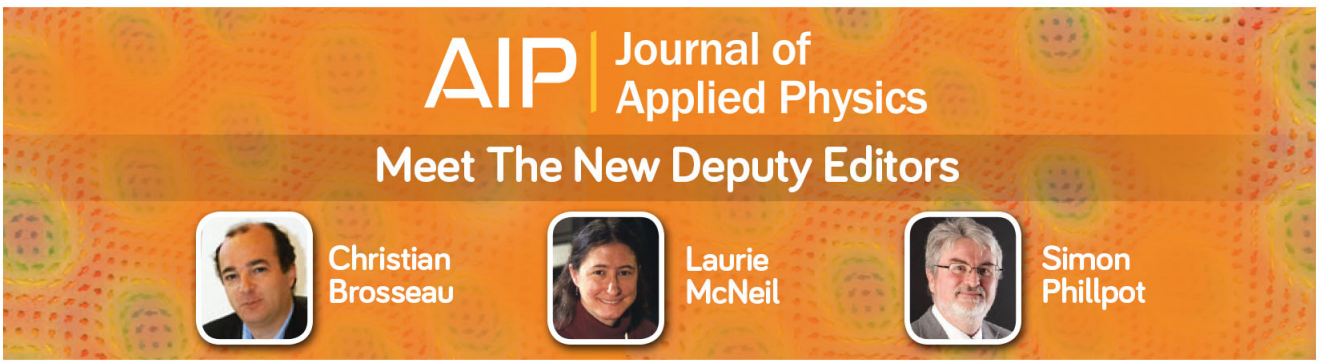

Femtosecond laser-induced phase transformations in amorphous $Cu_{77}Ni_6Sn_{10}P_7$ alloy

Y. Zhang,[1] L. Liu,[1,2,a)] G. Zou,[1] N. Chen,[3] A. Wu,[1] H. Bai,[1] and Y. Zhou[1,4]
[1]*Department of Mechanical Engineering, Tsinghua University, Beijing 100084, China*
[2]*The State Key Laboratory of Tribology, Tsinghua University, Beijing 100084, China*
[3]*School of Materials Science and Engineering, Tsinghua University, Beijing 100084, China*
[4]*Department of Mechanical and Mechatronics Engineering, University of Waterloo, Waterloo, Ontario N2L 3G1, Canada*

(Received 18 September 2014; accepted 25 December 2014; published online 9 January 2015)

In this study, the femtosecond laser-induced crystallization of CuNiSnP amorphous ribbons was investigated by utilizing an amplified Ti:sapphire laser system. X-ray diffraction and scanning electronic microscope were applied to examine the phase and morphology changes of the amorphous ribbons. Micromachining without crystallization, surface patterning, and selective crystallization were successfully achieved by changing laser parameters. Obvious crystallization occurred under the condition that the laser fluence was smaller than the ablation threshold, indicating that the structural evolution of the material depends strongly on the laser parameters. Back cooling method was used to inhibit heat accumulation; a reversible transformation between the disordered amorphous and crystalline phases can be achieved by using this method. © *2015 AIP Publishing LLC*.
[http://dx.doi.org/10.1063/1.4905588]

I. INTRODUCTION

Recently, the application of femtosecond laser pulse for precision micromachining has been drawing great interests due to its ultrahigh processing speed.[1,2] Since laser-matter interactions depend strongly on the laser pulse duration, the penetration depth of thermal diffusion in the materials upon femtosecond laser irradiation is very limited, resulting in an extremely small heat-affected zone (HAZ). For example, after femtosecond laser radiation, aluminum showed a HAZ of less than 2 μm (Ref. 3) and nickel-based super alloys even showed a negligible HAZ accompanied by a 2 μm plastic deformation zone around the processed region.[4] This advantage makes femtosecond laser a promising tool for machining thermo-sensitive materials such as amorphous materials.

Amorphous thin film is widely used in magnetic devices, brazing filler metals, thin film transistors, etc., attributed to their unique mechanical, chemical, and physical properties.[5] In particular, the laser-induced reversible transformation between disordered amorphous and crystalline phases is extremely advantageous in optical data storage.[6] Despite this, the studies on the interaction between femtosecond laser and amorphous materials are very limited in the literature. Femtosecond laser can also be a good tool to reduce the thickness of amorphous $Ta_{42}Si_{13}N_{45}$ film without inducing crystallization.[7] Jia *et al*. found that there was a small crystallized region with nanometer-sized crystalline grains in the ablated zone formed by femtosecond laser pulses.[8] Zhang *et al*. also observed the crystallized micro-regions on the surface of amorphous $Ge_2Sb_2Te_5$ films with irradiation of femtosecond laser pulses.[9] In addition, femtosecond laser annealing can be used to induce spatially selective crystallization of the amorphous Si.[10]

Generally, the femtosecond laser manufacturing techniques associated with amorphous materials can be divided into three types: surface micromachining or patterning without inducing crystallization,[11] selectively annealing/crystallization,[12] and selectively surface amorphization of crystal materials.[13] Therefore, utilizing femtosecond laser can either maintain the amorphous nature upon irradiation or induce reversible phase transformations between amorphous and crystalline phases. It is believed that the mechanisms for the three methods are different. However, many factors such as laser parameters, micromachined materials, and examination methods in the research conducted in the literature need to be taken into account, making it difficult to figure out the real mechanisms.

In the present study, a 50 fs Ti: sapphire laser was used to irradiate the amorphous $Cu_{77}Ni_6Sn_{10}P_7$ ribbons. We investigated the effects of laser parameters (such as laser power, focal condition, and scanning speed) on the phase changes of the amorphous alloy in details. The mechanism responsible for the interaction between femtosecond laser and amorphous ribbons was discussed. The process parameters were proposed to control annealing and selective area machining of the amorphous ribbons. Furthermore, a reversible transformation between amorphous and crystallization has been successfully realized in these Cu-based amorphous ribbons.

II. EXPERIMENTAL PROCEDURE

In the present experiment, samples were processed by an amplified Ti: sapphire laser system (Coherent Inc.) generating 50 fs pulses with a maximum energy of about 3.8 mJ per pulse at 1 kHz repetition rate. The laser emits linearly polarized pulses at a central wavelength of 800 nm with Gauss beam distribution. The experiments were carried out in air. The laser beam has an 8 mm diameter, and was

a)Electronic mail: liulei@tsinghua.edu.cn

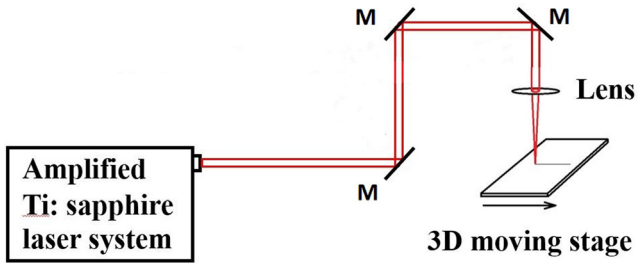

FIG. 1. Schematic diagram of the experience light path.

focused by a 25.4 mm-focal-length lens, the diameter of the focal point was about 50 μm. Commercially available amorphous $Cu_{77}Ni_6Sn_{10}P_7$ alloy ribbons were used as the original materials for laser irradiation tests, which were provided by Nanostructured & Amorphous Materials, Inc. (Houston, TX). All samples of the as-quenched ribbons have dimensions of 20 mm × 20 mm × 30 μm.

Differential scanning calorimetry has been used to measure the glass transition temperature (T_g), crystallization temperature (T_x), and the melting temperature (T_m) of the CuNiSnP amorphous ribbons. The schematic diagram of the light path is shown in Fig. 1. The samples were moved perpendicular to the beam with different defocus positions, laser powers, and scanning velocities. The microstructure of the samples was tested by a micro-area X-ray diffraction (XRD) (RigakuR-AxisSpider) using *Mo Kα* radiation at 50 kV and 80 mA, the test scope is $0.8 \times 0.8\ mm^2$. Surface appearance was observed by a scanning electronic microscope (SEM) with a model of LEO 1530.

The offset amount between laser focused position and sample plane is defined as dF, which is tuned by a computer-controlled motion stage with a resolution of 0.1 μm. Single pulse fluence or laser fluence, defined as F = E/nA, and number of laser pulse is used to characterize the induced laser radiation, where E is the laser power, n is the number of the pulses, and A is the laser focus area on the sample. By changing dF and E, different laser fluences can be acquired.

III. RESULTS AND DISCUSSION

As we can see from the DSC curve shown in Fig. 2, the glass transition reaction, which is an endothermic reaction, started at 175 °C, where the heat flow of $Cu_{77}Ni_6Sn_{10}P_7$ ribbon slightly decreased with the increasing of temperature at 175 °C (T_g). Crystallization occurred at 200 °C (T_x), where a heat flow peak appeared. The amorphous ribbon started melting at 600 °C (T_m) and ended at 643 °C (T_l), respectively.[14] The supercooled liquid region ΔT defined as a difference between T_x and T_g is an indicator for the thermal stability of the amorphous structure.[15] In the case of the $Cu_{77}Ni_6Sn_{10}P_7$ ribbons, the ΔT is only 25 °C, suggesting that the $Cu_{77}Ni_6Sn_{10}P_7$ ribbons are thermally sensitive.

When heating the as-quenched amorphous ribbons in vacuumed oven to 250 °C and holding for 10 min, the samples were fully crystallized in the equilibrium phases as shown in Fig. 3. Cu_3P, Cu_3Sn, and Cu_9NiSn_3 are the crystalline phases during this thermal activated process.

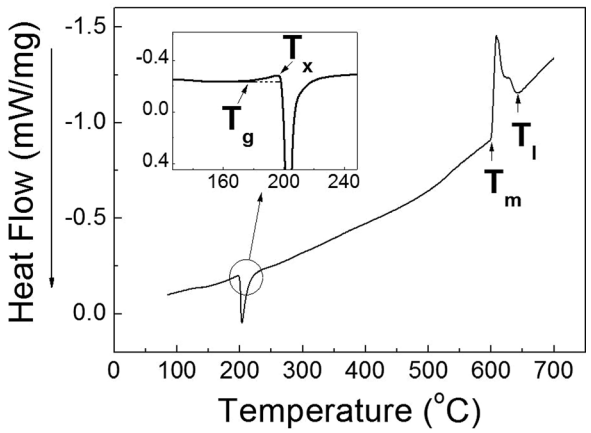

FIG. 2. DSC curve of the CuNiSnP alloy ribbons. The heating rate was 10 °C/min.

Fig. 4 shows the XRD results of the as-quenched ribbons and the ones scanned at different laser fluences. The as-quenched ribbons present a broad diffuse peak with 2θ ranging from 34° to 44°, typically for amorphous alloys when the laser fluence was 4.14 J/cm^2. Similarly, a broad diffuse peak at around 2θ = 34°–44° was also observed. However, the first diffuse peak for the ribbons irradiated by the laser fluence of 4.14 J/cm^2 tapers to a sharp point (2θ = 41.0°) in the center. The tapered point was close to Cu_3P diffuse peak (2θ = 40.6°), which could be the first crystalline phase precipitating in the amorphous matrix, suggesting crystallization occurred after femtosecond laser irradiation. As laser fluence decreased to 0.23 J/cm^2, diffraction peaks with narrow FWHM values (full width at half maximum) appeared, indicating that the scanned region of the specimen was almost fully crystallized. Those peaks were identified as Cu_3P, Cu_3Sn, and Cu_9NiSn_3. When further reducing the laser fluence to 0.12 J/cm^2, the crystallization of the amorphous ribbons was accomplished more thoroughly even than that irradiated by the laser fluence of 0.23 J/cm^2. Upon laser irradiation with a laser fluence of 0.03 J/cm^2, the amorphous ribbons slightly crystallize, similar to that with a laser fluence of 4.14 J/cm^2. Comparing to Fig. 3, we can indicate that the

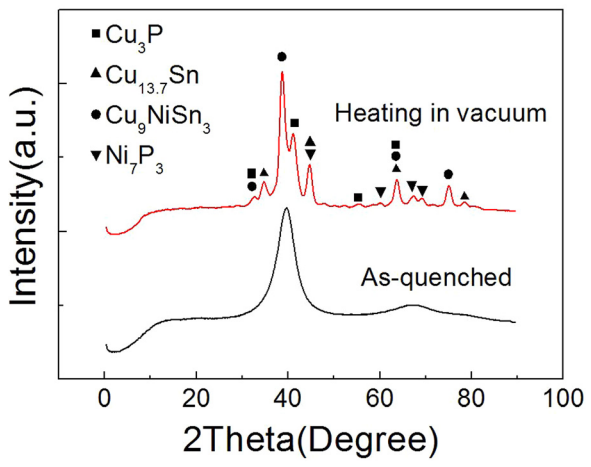

FIG. 3. XRD results of samples crystallized in vacuumed oven.

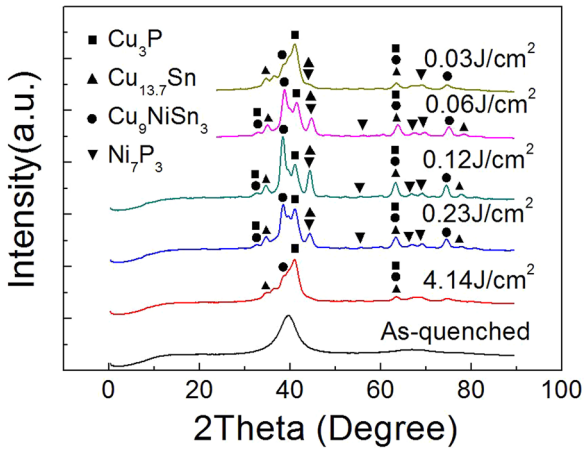

FIG. 4. XRD results of samples scanned at different laser fluences.

crystallization induced by both annealing and laser irradiation (the fluence of the laser was 0.12 J/cm^2) is a thermal activated process, thus yielding the same crystalline phases.

Fig. 5 shows the SEM images of the as-quenched ribbons and the samples scanned with different laser fluence. The as-quenched ribbons exhibit a smooth surface as shown in Fig. 5(a). Under laser irradiation, the surface morphology evolves with increasing the laser fluence from 0.03 J/cm^2 to 4.14 J/cm^2. At the lowest laser fluence of 0.03 J/cm^2, a porous surface with nanometer-sized pores was formed as indicated in Fig. 5(b). Increasing the laser fluence to 0.23 J/cm^2, micro-scale periodical textures appeared on the specimen surface (Fig. 5(c)). The composition of the texture surface was measured by EDA (energy dispersive analysis) and listed in Table I. It was found that Ni, Sn, and P contents were reduced after laser irradiation. Further increasing laser fluence to 4.14 J/cm^2 enables formation of submicron ripples in the middle of the exposed surface with nanoparticles dispersing in the irradiated zone (Fig. 5(d)).

Fig. 6 shows the optical microscope images of the cross section of the specimen processed under the laser influence

TABLE I. Composition changes during laser irradiation.

Elements (at %)	P K	Ni K	Cu L	Sn L
Point A	11.72	3.14	81.37	3.77
Point B	5.87	1.71	90.62	1.89

of 0.23 J/cm^2. The shape and the width of the ripples are clearly shown in the cross section image. Because of the Gaussian energy distribution of the laser beam, the center part of the sample formed higher ripples, where absorb more laser energy, the edge part of the sample formed shorter ripples, where absorb less energy.

When laser is exposed on the surface of the amorphous material, the energy can be divided into three parts: the first part of the energy is reflected by the material; the second part is absorbed by the base metal and induces melting or annealing;[16,17] the third part induces ablation and vaporization.[18]

When the laser fluence was 4.14 J/cm^2, the film was cut off, indicating that the fluence was above the ablation threshold. The atoms were quickly heated to above vaporization temperature before the heat transfers to the surrounding material.[19]

When the laser fluence was 0.23 J/cm^2, the thickness of the sample after irradiation slightly reduced by about 7 μm (in Fig. 6), suggesting that the laser fluence was below the ablation threshold. The surface became rougher (as shown in Fig. 5(c)) and the absorption rate was enhanced,[20] a considerable amount of laser energy was deposited on the amorphous film[2] and induced crystallization. When the laser influence was further down to 0.03 J/cm^2, both ablation and crystallization were hard to occur due to an insufficient energy input.

Fig. 7 shows the XRD results of the samples processed by different pulse numbers. As shown in Fig. 7, the FWHM values of the diffraction peaks decrease as the pulsed numbers increase, indicating that more material crystallized with

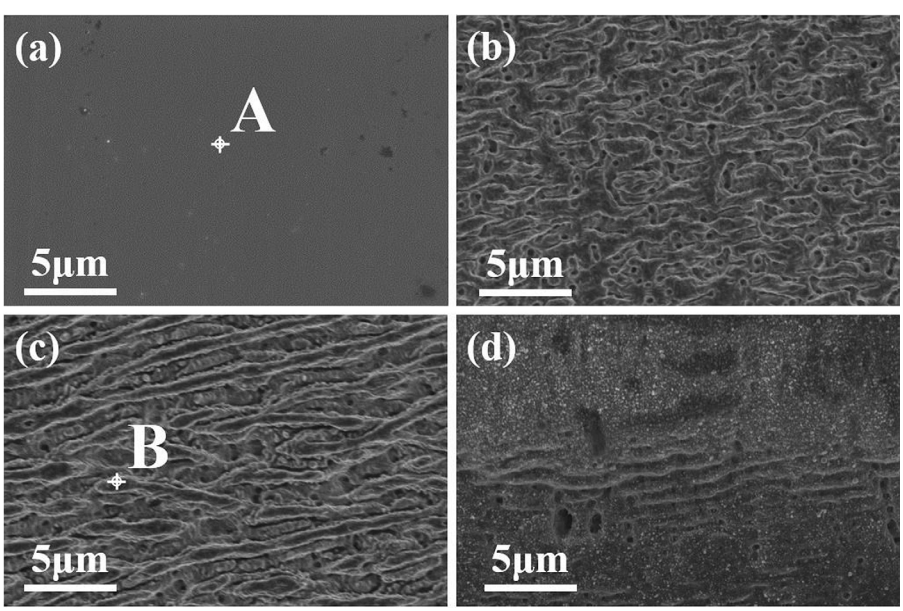

FIG. 5. The top surface SEM images of the amorphous samples in an as-prepared state (a) and scanned at different laser fluence (b) 0.03 J/cm^2, (c) 0.23 J/cm^2, and (d) 4.14 J/cm^2.

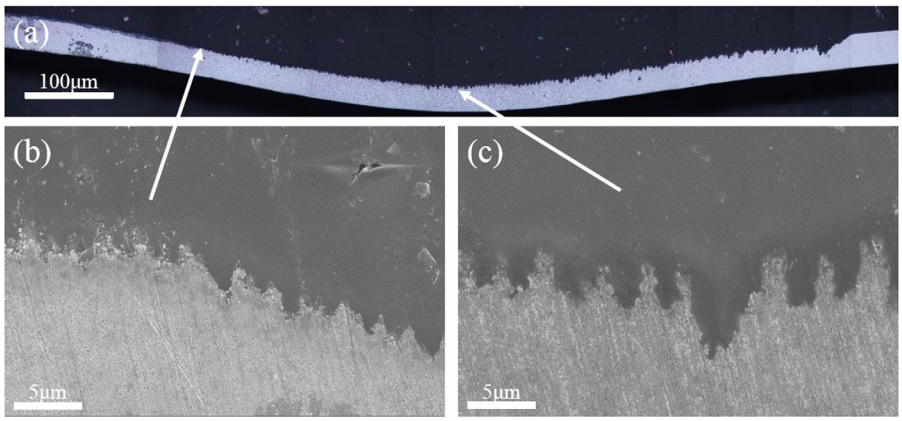

FIG. 6. (a) Optical microscope picture of cross section of specimen. Laser fluence was 0.23 J/cm^2; (b) SEM picture at edge part of the specimen; (c) SEM picture at center part of the specimen.

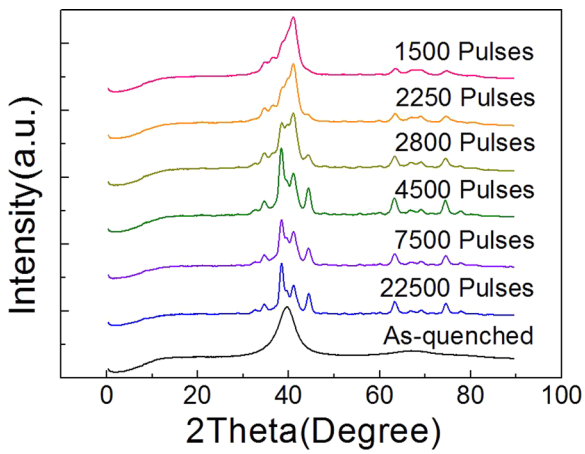

FIG. 7. XRD results of samples processed by different pulse numbers.

more pulses irradiated on the sample. As mentioned in the study of Weber *et al*., the heat accumulation could be larger with more pulse numbers, even when the single pulse energy was lower.[21] Therefore, laser pulse number can also pose an effect on the degree of crystallization.

Fig. 8 shows the SEM images of the sample surfaces processed by different pulses numbers. It can be observed that as the pulse number increases, the surface becomes rougher. Combining Figs. 7 and 8, the microstructural evolution of the sample versus number of pulses could be summarized as three stages: (1) submicron scale pores appeared in 1500 pulses and slight crystallization was induced; (2) more submicron scale pores appeared in 2800 pulses and obvious crystallization was induced; (3) as the pulse number increases, the surface became rougher and the energy absorption rate was enhanced. Since the energy density was below the ablation threshold, most of the laser energy transferred into heat and induced the complete crystallization of the sample.

The above results indicate that when ablation occurred, the heat effect of femtosecond laser was very small. However, if the laser energy density was below the ablation threshold, heat effects were not neglectable anymore. The extent of crystallization induced by femtosecond laser was strongly related to the pulse number, which determines the heat accumulation and the surface roughness. Rougher surface can enhance the absorption rate, which was proved by former experiments. In order to check the effect of heat accumulation on crystallization, a copper plate was placed on the back side of the amorphous ribbons to increase the heat dissipation. After laser irradiation, when the sample was scanned with the copper cooling plate, no sharp peaks appear in the curve, whereas the one was scanned under air cooling condition, sharp diffraction peaks appear, as shown in Fig. 9.

A model of laser absorption has been given in Fig. 10, which was similar to the model summarized by Bonse *et al*.[22] Ablation occurred and took away most part of the laser energy. The residue energy caused melting of the surrounding materials, which was also observed by others (melting thickness was 500 nm reported by Jia *et al*.[8]). Because the thermal capacity is restricted by the amorphous film thickness (only 30 μm), the residue heat transferred to the annealing zone and caused slight crystallization due to multipulse heat accumulation. The trend of crystallization was evidenced by XRD curves in Fig. 4. When a thick copper plate (3 mm) was placed under the amorphous film, the residue heat dissipated to the copper. The melted materials were quenched and annealing effect was inhibited due to no heat accumulation, resulting in no crystallization occurring and the film staying as amorphous structures.

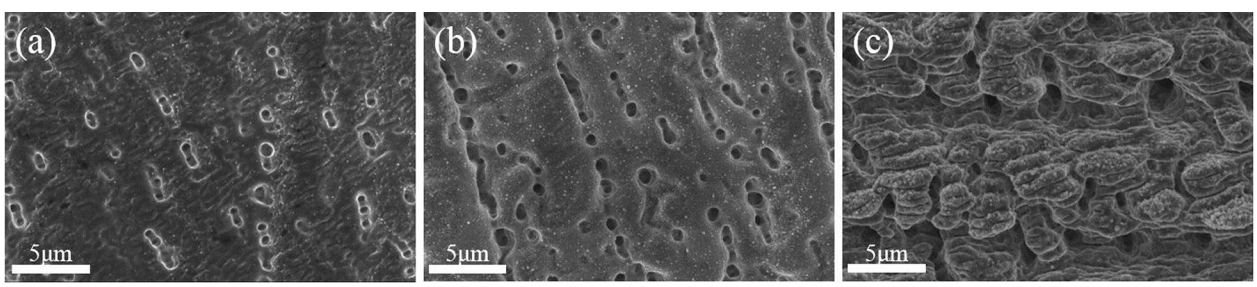

FIG. 8. SEM pictures of samples surface processed by different pulses numbers: (a) 1500 pulses, (b) 2800 pulses, and (c) 7500 pulses.

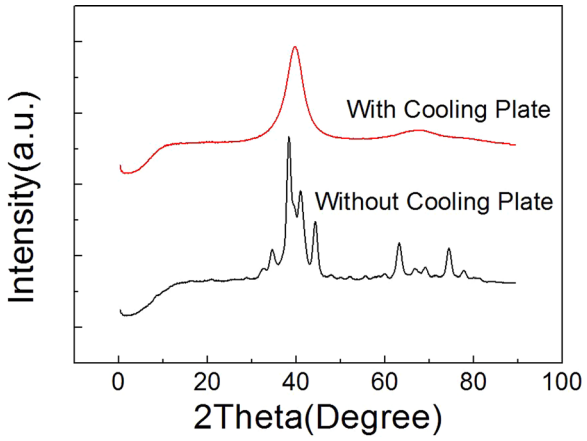

FIG. 9. XRD results of samples processed by femtosecond laser when copper back cooling plate was used.

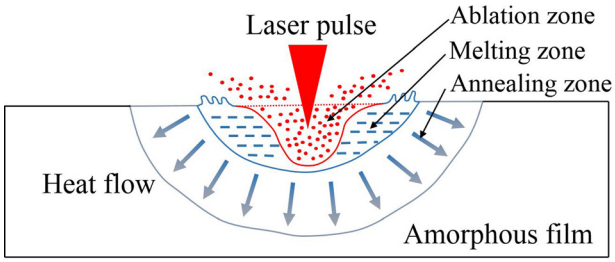

FIG. 10. Schematic diagram of the laser irradiation process.

By using this method, we also tried to amorphize the crystallized sample. The experiment was done in two steps. At first, the sample was crystallized by femtosecond laser with the laser fluence of 0.12 J/cm^2 as shown in Fig. 11. Consequently, a back copper plate was used to increase the heat dissipation, and the laser with the same parameters was used to scan at the same position of the sample. The crystallized sample was amorphized again. Utilizing femtosecond laser, the transformation between crystallization and amorphization of an amorphous alloy is reversible, which is important for micromachining and manufacturing amorphous materials and structures.

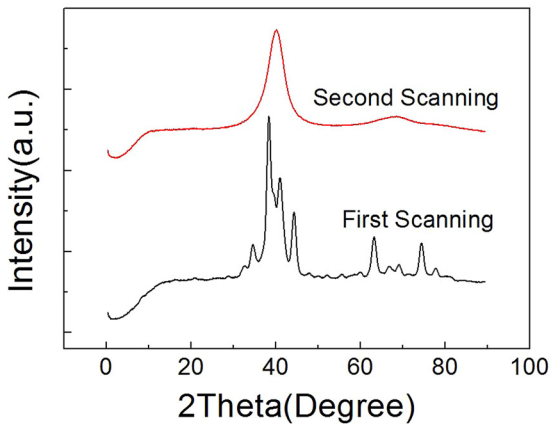

FIG. 11. XRD results of sample scanned by two-step method.

IV. CONCLUSIONS

In this study, femtosecond laser was used to selectively crystallize the amorphous ribbons, micromachine and pattern the amorphous ribbons without crystallization. The main conclusions are as follow:

(1) The heat effect of femtosecond laser can induce crystallization of amorphous CuNiSnP alloy. At a low laser fluence of 0.03 J/cm^2, the first crystalline Cu_3P phase appears. Further increasing the laser fluence to 0.23 J/cm^2 promotes formation of multi-crystalline phases.
(2) The heat effect of femtosecond laser was determined by the laser influence and the pulse number. When the laser fluence was above the ablation threshold, only slight crystallization can be observed. When the laser fluence was below the ablation threshold, obvious crystallization occurred. With increasing the pulse number, the surface becomes rougher and more crystallization were observed, which was because of the enhanced laser absorption rate and heat accumulation.
(3) Back cooling can effectively inhibit the heat accumulation and keep the ribbons remain in their amorphous state. By using back cooling method, a reversible transformation between the amorphous and crystalline phase can be achieved.

ACKNOWLEDGMENTS

This work was supported by National Natural Science Foundation of China (Grant Nos. 51375261 and 51405258), by The Natural Science Foundation of Beijing (Grant No. 3132020), by The Specialized Research Fund for Doctoral Program of Higher Education (Grant No. 20130002110009), and by Tsinghua University Initiative Scientific Research Program (Grant Nos. 2010THZ 02-1 and 2013Z02-1).

[1]L. Liu, P. Peng, A. Hu *et al.*, Appl. Phys. Lett. **102**, 073107 (2013).
[2]A. Y. Vorobyev and C. Guo, Laser Photonics Rev. **7**, 385 (2013).
[3]R. Le Harzic, N. Huot, E. Audouard *et al.*, Appl. Phys. Lett. **80**, 3886 (2002).
[4]Q. Feng, Y. N. Picard, H. Liu *et al.*, Scr. Mater. **53**, 511 (2005).
[5]N. Chen, D. V. Louzguine-Luzgin, G. Q. Xie *et al.*, Nanotechnology **24**, 045610 (2013).
[6]H. Lu, E. Thelander, J. W. Gerlach *et al.*, Adv. Funct. Mater. **23**, 3621 (2013).
[7]V. Romano, M. Meier, N. D. Theodore *et al.*, Appl. Phys. A **104**, 357 (2011).
[8]J. Jia, M. Li, and C. V. Thompson, Appl. Phys. Lett. **84**, 3205 (2004).
[9]G. Zhang, D. Gu, F. Gan *et al.*, Thin Solid Films **474**, 169 (2005).
[10]G. J. Lee and Y. Lee, J. Korean Phys. Soc. **53**(1), 1414–1418 (2008).
[11]G. J. Lee, J. Park, E. K. Kim *et al.*, Opt. Express **13**(17), 6445 (2005).
[12]O. Salihoglu, U. Kürüm, H. G. Yaglioglu *et al.*, J. Appl. Phys. **109**, 123108 (2011).
[13]Y. Izawa, Y. Setuhara, M. Hashida *et al.*, Jpn. J. Appl. Phys., Part 1 **45**(7), 5791 (2006).
[14]W. Chen, Y. Wang, J. Qiang *et al.*, Acta Mater. **51**(7), 1899–1907 (2003).
[15]A. Inoue, N. Nishiyama, and H. Kimura, Mater. Trans., TIM **38**(2), 179–183 (1997).
[16]A. Y. Vorobyev and C. Guo, Phys. Rev. B **72**, 195422 (2005).
[17]A. Y. Vorobyev and C. Guo, Appl. Phys. Lett. **86**, 011916 (2005).
[18]W. Jia, D. Zhang, X. Li *et al.*, Thin Solid Films **516**, 2260–2263 (2008).
[19]R. Gattass and E. Mazur, Nat. Photonics **2**, 219–225 (2008).
[20]A. Y. Vorobyev and C. Guo, Proc. SPIE **7005**, 70051T (2008).
[21]R. Weber, T. Graf, P. Berger *et al.*, Opt. Express **22**(9), 11312 (2014).
[22]J. Bonse, S. Baudach, J. Kruger *et al.*, Appl. Phys. A **74**, 19–25 (2002).